







Detection of a new GeV source in the outer region of the Coma cluster: a signature of external accretion shock ?

XIAO-BIN CHEN ^{1,2} KAI WANG ^{3,2} YI-YUN HUANG ^{3,2} HAI-MING ZHANG ⁴ SHAO-QIANG XI⁵ RUO-YU LIU ^{3,2}
AND XIANG-YU WANG ^{3,2}

¹*School of Astronomy and Space Science, Nanjing University, Nanjing 210023, China; xywang@nju.edu.cn; xbc@smail.nju.edu.cn*

²*Key laboratory of Modern Astronomy and Astrophysics (Nanjing University), Ministry of Education, Nanjing 210023, China*

³*School of Astronomy and Space Science, Nanjing University, Nanjing 210023, China*

⁴*Guangxi Key Laboratory for Relativistic Astrophysics, School of Physical Science and Technology, Guangxi University, Nanning 530004, China*

⁵*Key Laboratory of Particle Astrophysics & Experimental Physics Division & Computing Center, Institute of High Energy Physics, Chinese Academy of Sciences, 100049 Beijing, China*

ABSTRACT

The supersonic flow motions associated with infall of baryonic gas toward sheets and filaments, as well as cluster mergers, produces large-scale shock waves. The shocks associated with galaxy clusters can be classified mainly into two categories: internal shocks appear in the hot intracluster medium within the virial radius, and external accretion shocks form in the outer cold region well outside of the virial radius. Cosmic-ray (CR) electrons and/or protons accelerated by these shocks are expected to produce gamma-rays through inverse-Compton scatterings (ICS) or inelastic pp collisions respectively. Recent studies have found a spatially extended GeV source within the virial radius, consistent with the internal shock origin. Here we report the detection of a new GeV source at a distance of about 2.8° from the center of the Coma cluster through the analysis of 16.2 years of Fermi-LAT data. The hard spectrum of the source, in agreement with the ICS origin, and its location in a large-scale filament of galaxies points to the external accretion shock origin. The gamma-ray ($0.1 - 10^3$ GeV) luminosity of the source, 1.4×10^{42} erg s⁻¹, suggests that a fraction $\sim 10^{-3}$ of the kinetic energy flux through the shock-surface is transferred to relativistic CR electrons.

Keywords: Galaxy clusters (584) — Shocks (2086) — Cosmic rays (329)

1. INTRODUCTION

Galaxy clusters, the largest gravitationally bound structures in the Universe, are thought to form through mergers and accretion of smaller structures. The supersonic flow motions associated with cluster mergers and accretion naturally induce shocks, which have been extensively studied using cosmological hydrodynamic simulations (Miniati et al. 2000; Ryu et al. 2003; Pfrommer et al. 2006; Ha et al. 2023). The shocks can be classified mainly into two categories (Ryu et al. 2003). One is internal shocks that appear in the hot ($T \sim 10^8$ K) intracluster medium (ICM) within the virial radius as the merging components approach each other at slightly supersonic speed. Another is external accretion shocks that form in the outer region well outside of the virial radius, where the cold ($T \sim 10^4$ K) gas in void regions and the warm-hot ($T \sim 10^5 - 10^7$ K) intergalactic medium in filaments accrete onto clusters. Accretion shocks are typically much stronger with highly supersonic speed since they develop in cold external cluster regions. As for typical astrophysical shocks, these cosmological shocks are collisionless, and hence are expected to accelerate cosmic ray (CR) protons and electrons to very high energies via diffusive shock acceleration (Loeb & Waxman 2000). Interactions between CR particles and the ambient medium, radiation, and magnetic fields may generate nonthermal emission in a wide range of wavelengths.

The Coma cluster of galaxies is the nearest massive clusters at a distance of ~ 100 Mpc. It shows evidence of efficient particle acceleration, as suggested by the presence of a giant radio halo and radio relics (Thierbach et al. 2003; Brown & Rudnick 2011; van Weeren et al. 2019). Fermi Large Area Telescope (Fermi-LAT) collaboration found two low-significance structures within the virial radius of the Coma cluster using 6 yr data (Ackermann et al. 2016). Xi

et al. (2018) reported the discovery of significant GeV gamma-ray emission from the Coma cluster with an unbinned likelihood analysis of the 9 years of Fermi-LAT data. For the first time, they also found tentative evidence that the gamma-ray emission is spatially extended. Later works with more data and detailed analyses (Adam et al. 2021; Baghmany et al. 2022) confirmed that a significant gamma-ray signal is observed roughly within the virial radius of the Coma cluster and the source is spatially extended. This gamma-ray source is located within the virial radius, consistent with the internal shock origin.

Nonthermal emission in the outer region of galaxy clusters beyond the virial radius has long been postulated as direct evidence for CR acceleration at external accretion shocks (Keshet et al. 2003; Ryu et al. 2003). Theoretically, it is expected that gamma-ray emission is dominated by the hadronic process in the cluster core region, whereas in the outskirts region the IC emission is the dominant component (Miniati et al. 2001; Pinzke & Pfrommer 2010). In particular, gamma-ray (Loeb & Waxman 2000; Totani & Kitayama 2000; Scharf & Mukherjee 2002; Keshet et al. 2003; Miniati 2003; Pinzke & Pfrommer 2010) and hard X-ray radiation (Enßlin et al. 1999; Kushnir & Waxman 2010) could possibly be produced by the inverse-Compton (IC) scattering of cosmic microwave background (CMB) photons off CR electrons accelerated at accretion shocks. Radio synchrotron radiation could also originate from accretion shocks as well (Bonafede et al. 2022). Although a few studies found preliminary evidence for a large gamma-ray ring around the Coma cluster from the VERITAS mosaic and Fermi-LAT data (Keshet et al. 2017; Keshet & Reiss 2018), more clear observational evidence would be required to firmly support CR acceleration at accretion shocks. In this *Letter*, we report the detection of a gamma-ray source in the outer region of the Coma cluster at a statistic significance of $\sim 5\sigma$ by using 16.2 years of Fermi-LAT data. The spatial position and spectral/morphological properties of the source suggest accretion shock as the origin of the gamma-ray emission.

The rest part of the paper is organized as follows. We present a description of the data analysis and show the morphological and spectral results of the new gamma-ray source in Section 2. Then we discuss the accretion shock origin of the source in Section 3. Finally, we give conclusions and discussions in Section 4.

2. FERMI-LAT DATA ANALYSIS

2.1. Data selection and background models

We used 16.2 yr of Fermi-LAT data from August 2008 to October 2024 to study the GeV emission near Coma cluster. The event class `P8R3_ULTRACLEANVETO` (evclass = 1024) and event type `FRONT + BACK` (evtpye = 3) are used. This is the cleanest Pass 8 event class and recommended to check for extra-galactic diffuse analysis¹. To account for the diffuse emission, we modelled the Galactic diffuse emission model (`gll_iem_v07.fits`) with isotropic component (`iso_P8R3_ULTRACLEANVETO_V3_v1.txt`) relevant to the `ULTRACLEANVETO` event class. We use recommended time selection of `(DATA_QUAL > 0) && (LAT_CONFIG == 1)`. To minimize the contamination from the Earth limb, the maximum zenith angle is set to be 90° .

The data selection was within a region of interest (ROI) of 20° around the center of the Coma cluster at (R.A., Dec.) = $(194.95^\circ, 27.98^\circ)$ with an energy range between 100 MeV and 1 TeV. We include the Galactic diffuse emission (GDE), isotropic emission and all sources listed in the fourth Fermi-LAT catalog (Ballet et al. 2023) in the background model. All sources within 6° of the center, as well as the GDE and isotropic emission components, are left free. The maximum likelihood test statistic (TS) is used to estimate the significance of gamma-ray sources, which is defined by $TS = 2(\ln\mathcal{L}_1 - \ln\mathcal{L}_0)$, where $\ln\mathcal{L}_1$ and $\ln\mathcal{L}_0$ are maximum likelihood values for the background with target source and without the target source (null hypothesis). In this work, the publicly available software *Fermitools* (v2.2.0) and the *Fermipy* tool (version 1.2.2) is used to perform the data analysis.

2.2. Morphological and spectral analysis

Based on the 4FGL catalog, there is a 4FGL point-like source, named 4FGL J1256.9+2736, that is roughly coincident with Coma cluster in position. The TS map is generated by removing this source from the background model. The resulted TS maps of the $8^\circ \times 8^\circ$ region are shown in Fig. 1 for 100 MeV–1 TeV, 100 MeV–500 MeV, and 500 MeV–1 TeV energy bands from left to right, respectively. In order to search for gamma-ray emission in the outer region of the Coma cluster, we have chosen a larger region of the Fermi-LAT data for the analysis than previously considered (Xi et al. 2018; Adam et al. 2021; Baghmany et al. 2022).

¹ https://fermi.gsfc.nasa.gov/ssc/data/analysis/documentation/Cicerone/Cicerone.Data.Exploration/Data_preparation.html

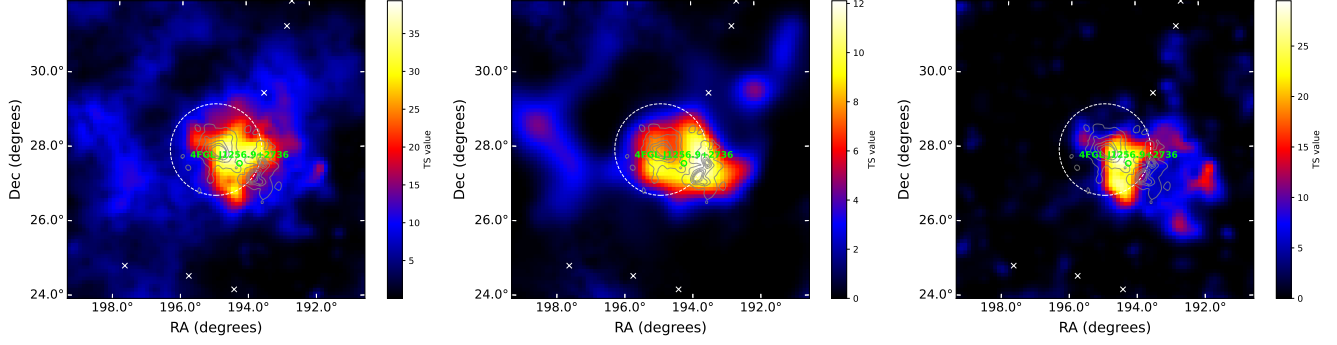


Figure 1. TS map of a $8^\circ \times 8^\circ$ region centered on the Coma cluster (left-hand panel: 100MeV–1TeV, middle panel: 100 MeV–500MeV, right-hand panel: 500MeV–1TeV). The dashed white circle represents the virial region of the Coma cluster ($\theta_{200} = 1.23^\circ$). The gray contours correspond to measurements of the Coma cluster using WSRT at a central frequency of 352 MHz (Brown & Rudnick 2011). The green circle shows the location of 4FGL J1256.9+2736 and the white crosses show the location of other 4FGL sources.

The morphology of the GeV emission is studied using the 4FGL J1256.9+2736 as the baseline model. We consider four spatial templates: (1) A point-like source (PS), i.e., 4FGL J1256.9+2736. We use the *Fermipy* tool to quantitatively reevaluate the location of this source. (2) The radio template. We consider a template assuming that the gamma-ray flux distribution traces the observed radio emission, since the radio emission traces relativistic electrons via synchrotron emission and could be associated with the gamma-ray signal. The radio emission template is based on the measurements of the Coma radio halo and relics using the Westerbork Synthesis Telescope (WSRT) at 352 MHz by Brown & Rudnick (2011). (3) A disk template. The best-fitted center of the disk is located at (R.A., Dec.) = $(194.25^\circ \pm 0.15^\circ, 27.56^\circ \pm 0.17^\circ)$ and the best-fitted extension is $R_{68} = 0.89^\circ \pm 0.11^\circ$. Here, we use the *extension* tool in *Fermipy* to measure the position and size of the extended source². This tool computes TS of the extension hypothesis defined as $\text{TS}_{\text{ext}} = 2 \times (\log \mathcal{L}_{\text{ext}} - \log \mathcal{L}_{\text{PS}})$, where $\log \mathcal{L}_{\text{ext}}$ and $\log \mathcal{L}_{\text{PS}}$ are likelihood values of the extended and point-like source models, respectively. We found that the extension TS value of the disk model is $\text{TS}_{\text{ext}} = 28.046$. (4) A Gauss template. The best-fitted center of the disk is located at (R.A., Dec.) = $(194.29^\circ \pm 0.16^\circ, 27.73^\circ \pm 0.16^\circ)$ and the best-fitted extension is $R_{68} = 0.89^\circ \pm 0.19^\circ$ with $\text{TS}_{\text{ext}} = 26.100$. Compared with the point-like source model, all of the disk, Gauss model and radio emission model improve the fitting significantly (see Table 1 for more details), which is consistent with previous analysis (Xi et al. 2018; Adam et al. 2021; Baghmanyan et al. 2022). Since the disk template has the best improvement on likelihood, our subsequent analysis will be based on this template.

Besides the gamma-ray emission presented above, which is within the viral radius θ_{200} (here the subscript 200 refers to an enclosed density 200 times above the critical density of the Universe) of the Coma cluster, we found that there is a significant excess to the west of this extended source, about 2.8° from the Coma cluster, particularly evident in the 500 MeV–1 TeV map. In Figure 2, we present the residual map after subtracting the disk component from Coma cluster in the 500 MeV–1 TeV range, showing the presence of residual emission. Therefore, we tested a two-component model, adding a point-like source to the original disk model. The best-fitted position of the new point-like source is (R.A., Dec.) = $(191.772^\circ \pm 0.035^\circ, 27.465^\circ \pm 0.045^\circ)$. We find that the TS value is increased by $\Delta\text{TS} \simeq 26$ for the disk plus a point-like source model compared to the single disk model (see Table 1), supporting the presence of an additional gamma-ray source at a statistic significance of about 5σ (hereafter, we name the point-like source as the source “W”). To assess the robustness of this additional source, we investigate how the detection significance of the source W changes in the systematic checks. The TS value of the source ranges from 23.5 to 28.4 (see Appendix A for more details). To test the extension of the source W, we consider a uniform disk template to fit the source, but find that there is no improvement relative to the point-like source model. This could be due to the low significance of the source and the low Fermi-LAT angular resolution.

We examine whether there is any known counterpart at the position of the source W. Since most of the high-latitude gamma-ray background sources are active galactic nuclei (AGNs) and they are sources of radio emission, we search for

² We avoided self-inconsistent results caused by program settings by customizing parameters, see as <https://github.com/fermiPy/fermipy/issues/555>

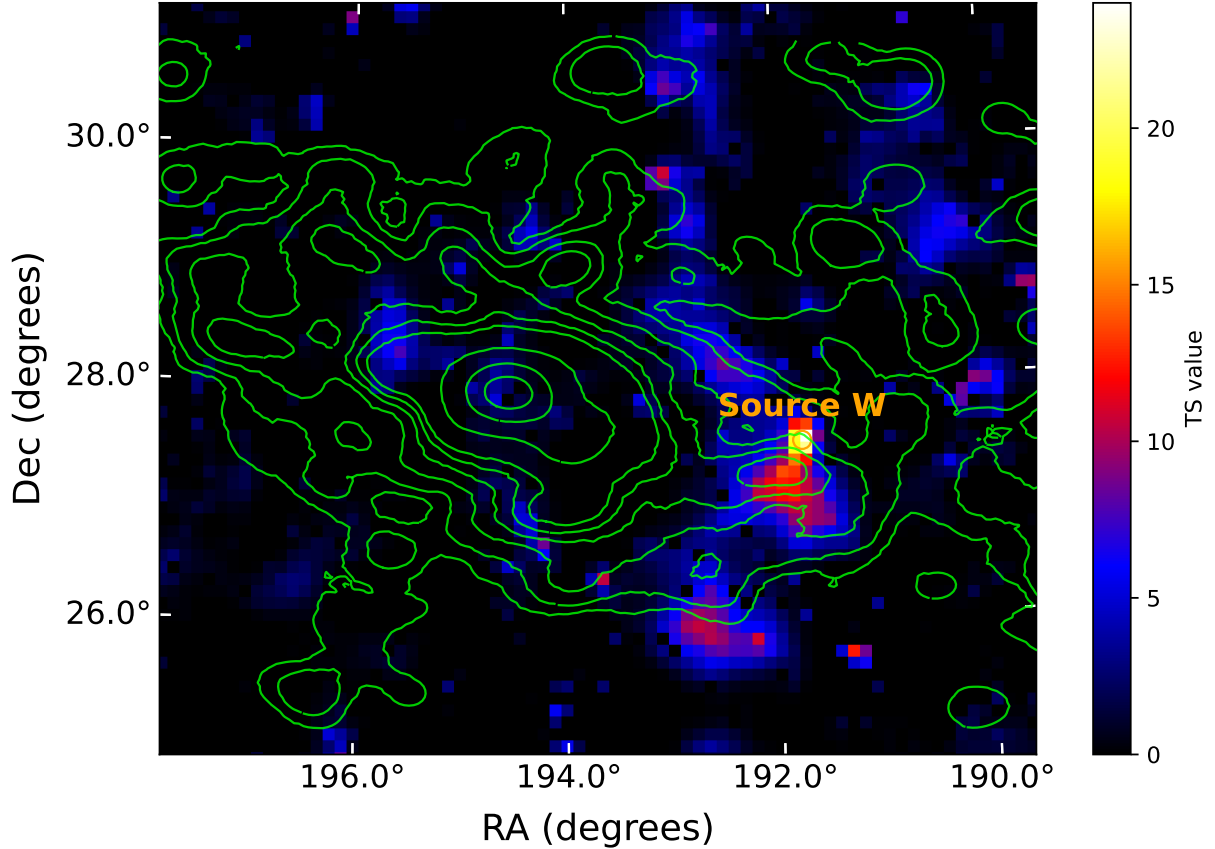


Figure 2. The residual map in 500 MeV-1 TeV of the Coma cluster region after subtracting the disk component in the core region. The green contours show the SDSS galaxy density distribution.

possible radio sources associated with the source W. We find no bright radio sources within 99% containment radius of the source W (see Appendix B for more details).

We compare the TS map of the gamma-ray source to the galaxy density distribution, as shown in Fig. 2. We select galaxies with spectroscopic information from the SDSS database³ and use this catalog to construct a galaxy density map around the Coma region (Adam et al. 2021). The source W is located in a galaxy filament in the west of the Coma cluster and is spatially coincident with a local overdensity of the galaxy distribution. Thus this source could be connected to the Coma cluster and its large-scale environment.

Considering the disk plus a point-like source template, we calculate the spectral energy distribution (SED) of the two components, which are shown in Fig. 3. Fitting with a power-law function, the photon index is $\alpha = -1.81 \pm 0.21$ for the point-like source component. The spectrum is quite hard compared with the gamma-ray emission from the disk component, whose photon index is -2.22 ± 0.11 . The hard spectrum motivate us to check the highest energy photons from the point-like source and find that two photons have energy of about 40 GeV and 110 GeV respectively. We use the `gtsrcprob` tool to obtain the probability of each photons coming from the point-like source in our model, which is shown in Table 2. The high probability of the association proves that the highest-energy photons belong to the point-like source and explain its hard spectrum. The energy flux of the disk component and the point-like source in 0.1–1000 GeV are respectively $(3.85 \pm 0.65) \times 10^{-12} \text{ erg cm}^{-2} \text{ s}^{-1}$ and $(1.20 \pm 0.58) \times 10^{-12} \text{ erg cm}^{-2} \text{ s}^{-1}$, leading to a total gamma-ray luminosity of $L_\gamma = (4.61 \pm 0.77) \times 10^{42} \text{ erg s}^{-1}$ and $L_\gamma = (1.44 \pm 0.69) \times 10^{42} \text{ erg s}^{-1}$ for the disk and point-like source, respectively.

We examine the flux variability of the source W by computing the light curves in four and eight time bins over 16.2 yr, for events in the energy range 0.1–1000 GeV. The result is shown in the Appendix C. We then use a likelihood-based

³ <https://skyserver.sdss.org/dr18>

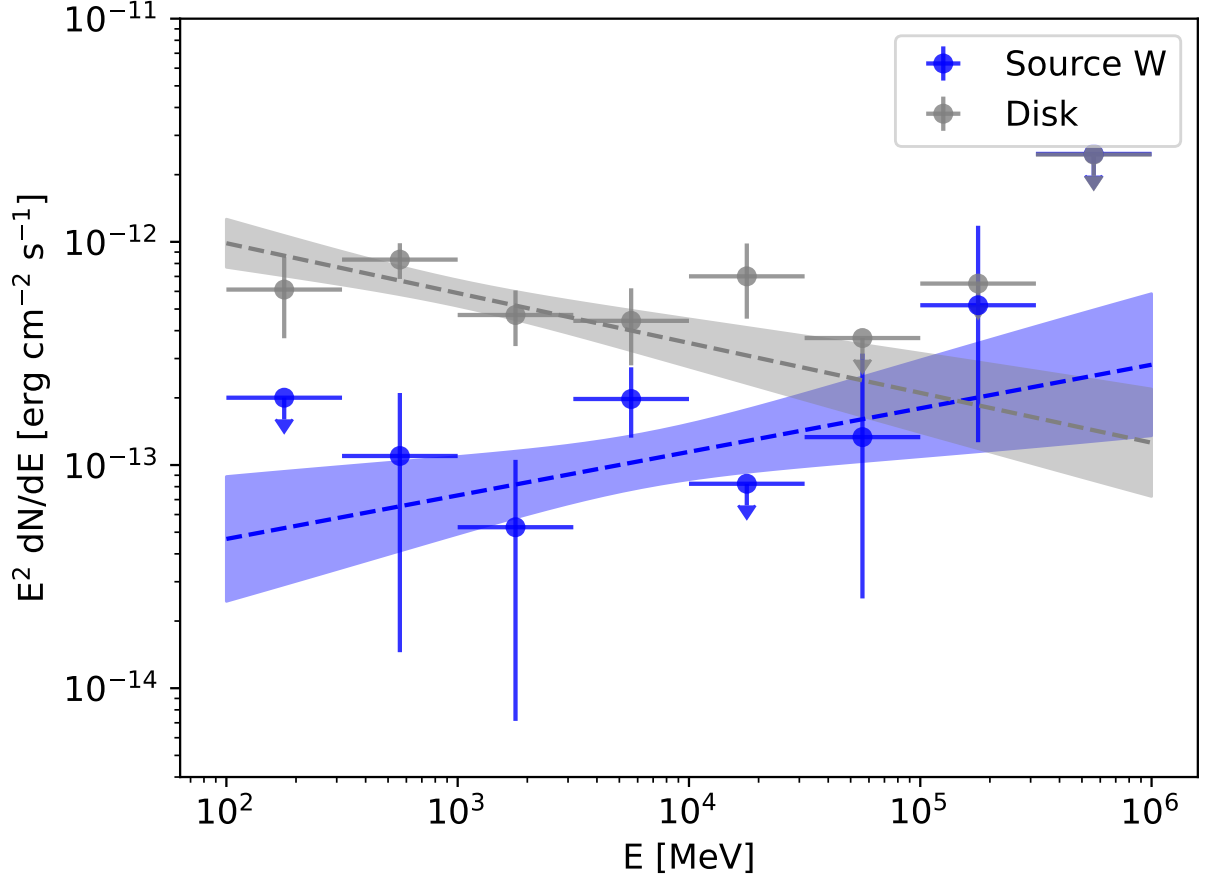


Figure 3. The spectral energy distribution (SED) of the disk component (in gray) and the point-like source component (in blue). The shaded areas mark the 1σ errors of the fitted spectral model.

Spatial model	Spectral index	TS	Δ TS
PS model	2.69 ± 0.17	29.11	-
Radio model	2.36 ± 0.13	47.26	15.56
Disk	2.22 ± 0.10	57.98	26.22
Gauss	2.21 ± 0.10	57.10	25.31
Radio model Source W	2.35 ± 0.13 1.81 ± 0.20	47.19 25.66	41.10
Disk Source W	2.22 ± 0.11 1.81 ± 0.20	59.98 25.48	52.02
Gauss Source W	2.22 ± 0.10 1.78 ± 0.21	60.54 24.61	47.45

NOTE— The Δ TS represents the improvement in the test statistic when comparing the fit of PS model (the first line) to alternative models.

Table 1. The result of the morphological analysis of the Coma cluster region in 100MeV-1TeV.

statistic to test the significance of the variability (Nolan et al. 2012). No evidence of the flux variability is found (see Appendix B for more details).

3. ACCRETION SHOCK ORIGIN FOR THE SOURCE W

Photon energy (MeV)	Source W	Galactic diffuse emission	Isotropic emission	Other sources
111456	96.5%	1.0%	2.4%	0.1%
43886	99.3%	0.2%	0.5%	0.0%

Table 2. The probability of association with various sources for the two highest energy photons from the direction of the source W.

The hard spectrum of the source W and its spatial coincidence with a local overdensity of the galaxy distribution suggest that it could result from an accretion shock. The accretion shock is characterized by high sonic velocity with a Mach number $M_s \gg 1$, and is expected to be efficient accelerators of cosmic ray protons and electrons. Due to a low gas density in the cluster outskirts ($n \sim 10^{-4} \text{cm}^{-3}$), the hadronic emission from the cosmic-ray protons is expected to be low, so the gamma-ray spectrum is dominated by the IC emission of primary CR electrons accelerated by accretion shocks. The energy distributions of CRs is described by a power-law function, $dN(E)/dE \propto E^{-p}$, with p determined by the shock Mach number M_s , which approaches $p = 2$ for $M_s \gg 1$ (Brunetti & Jones 2014). The cosmic-ray electrons can be accelerated up to energies of tens of TeV, and the resulting IC emission by scattering the CMB photons extends to multi-TeV (Keshet et al. 2003). These electrons lose a small fraction of energy into synchrotron emission since the magnetic field at the accretion shock is expected to be weak, $\leq 0.1 \mu\text{G}$. Because the cooling time of the GeV-emitting electrons (via the IC process), t_{cool} is short compared to the cluster dynamical time, $t_{\text{dyn}} \sim 1 \text{Gyr}$, these electron lose all their energy through IC emission during the dynamic time. Therefore, the resulting IC spectrum provides roughly equal energy flux per decade in photon energy for an electron spectrum with $p = 2$, i.e. $\nu F_\nu \propto \nu^0$ in the photon energy range 100 MeV-1 TeV. The measured spectral index ($\alpha = -1.81 \pm 0.21$) of the source W agrees with the predicted flat spectrum from the accretion shock model.

The gamma-ray emission from accretion shocks is expected to have an irregular morphology since the cooling time of these relativistic electrons is much shorter than the dynamic time of the cluster (Pfrommer & Jonathan Dursi 2010). The brightest region in the source W may correspond to a luminous peak where the accretion shock intersects the galaxy filament (Keshet et al. 2003). The kinetic energy flux through the surface of the accretion shock is $\dot{E}_k = 1/2 \rho V_{\text{sh}}^3 S$ (Brunetti & Jones 2014), where $\rho = nm_p$ is the the upstream gas density (n is the number density of the upstream gas and m_p is the proton mass), V_{sh} is the shock velocity and S is the shock surface area, respectively. Assuming that a fraction η_e of the kinetic energy flux through the shock-surface is transferred to relativistic cosmic-ray electrons, the total IC luminosity from CR is $L_{\text{IC}} \simeq 1/2 \eta_e \rho V_{\text{sh}}^3 S$.

The observed gamma-ray luminosity in 100 MeV-1 TeV is a fraction $\ln(10^4)/\ln(\gamma_{\text{max}}/\gamma_{\text{min}})$ of the total IC luminosity for a flat spectrum of $\nu F_\nu \propto \nu^0$. Taking $S = \pi R^2 = 2.8 \times 10^{49} \text{cm}^2$ (assuming $R \sim 1 \text{Mpc}$ for the size of the shock surface of the source W) and $\ln(\gamma_{\text{max}}/\gamma_{\text{min}}) = 20$, we obtain

$$\eta_e \simeq 10^{-3} \left(\frac{n}{10^{-4} \text{cm}^{-3}} \right)^{-1} \left(\frac{V_{\text{sh}}}{10^3 \text{km s}^{-1}} \right)^{-3} \left(\frac{R}{1 \text{Mpc}} \right)^{-2}. \quad (1)$$

This efficiency is consistent with the numerical simulation for accretion shocks (Ha et al. 2023). It also agrees with the inferred acceleration efficiency from the giant radio relics in some galaxy clusters (Brunetti & Jones 2014).

4. CONCLUSIONS AND DISCUSSIONS

Structure formation in the intergalactic medium produces large-scale, collisionless shock waves, in which electrons can be accelerated to highly relativistic energies. These electrons can produce gamma-ray emission through IC scatterings of the CMB photons. We reported the detection of such gamma-ray emission at the outer region of the Coma cluster. The hard spectrum of the excess emission, as well as its location in a large-scale filament of galaxies, are consistent with the accretion shock origin for the gamma-ray emission.

The IC emission could extend down to X-ray band as long as the power-law distribution of CR electrons extends to a minimum Lorentz factor of $\gamma_{\text{min}} \sim 10^3$. Assuming $\alpha = -1.81 \pm 0.21$ for the photon index, we expected a differential flux of $F_X \sim 10^{-14} - 10^{-13} \text{erg cm}^{-2} \text{s}^{-1}$ at X-ray band for the source W. Deep observations with NuSTAR, eROSITA and Einstein Probe could test this prediction.

The synchrotron radio emission of the source W can be estimated by $L_{\text{radio}} \sim L_\gamma (\frac{B}{B_{\text{CMB}}})^2$, where $B_{\text{CMB}} \equiv (8\pi T_{\text{CMB}}^4)^{1/2} = 3.2(1+z)\mu\text{G}$ is defined as the magnetic field for which the magnetic energy density equals the CMB energy density. Assuming $B \leq 0.1 \mu\text{G}$, we obtain $L_{\text{radio}} \leq 10^{-3} (B/0.1 \mu\text{G})^2 L_\gamma \sim 10^{39} \text{erg s}^{-1} (B/0.1 \mu\text{G})^2$. The radio emission of the source W could be also tested by sensitive radio observations in the future.

Type	Variation	Spectral index impact	Flux impact	Range of TS_{SourceW}
Diffuse modeling	Alt. diffuse models ^a	< 7%	< 15%	(24.55, 28.39)
Isotropic spectral template	Alt. isotropic models ^b	< 9%	< 20%	(23.52, 28.39)
Low-energy threshold	100–500 MeV	< 8%	< 10%	(23.53, 25.66)

^a `gll_iem_v07`, `gll_iem_v06` and 16 alternative background models discussed in Xi et al. (2018).

^b `iso_P8R3` for three event classes `SOURCE` (evclass = 128), `CLEAN` (evclass = 256) and `UNTRACLEANVETO` (evclass = 1024).

Table 3. Systematic uncertainties for the source W.

The work is supported by the NSFC under grants Nos. 12333006, 12121003 and 12203022.

APPENDIX

A. SYSTEMATIC UNCERTAINTIES

To assess the robustness of our results, we investigate how the detection significance of the source W changes in the systematic checks. We first study the impact caused by different low-energy thresholds of 100, 300, and 500 MeV. The spectral index and the detection significance of the source W change by less than 10%, primarily due to the hard spectral index of the source W.

Although Coma is located near the galactic north pole (i.e., in a very clean region regarding Galactic diffuse gamma-ray emission), the uncertainty from Galactic diffuse foreground modeling may still be significant. We thus compare results obtained by using the standard diffuse emission model with those obtained by using alternative diffuse emission models. Ackermann et al. (2012) provides 128 sets of maps corresponding to different model parameters. Following Xi et al. (2018), we adopt 16 sets among them, which varies in the most important parameters involved in creating the template, including CR source distribution (Lorimer, SNR), halo size (4, 10 kpc), spin temperature (150 K, 10^5 K), and E(B-V) magnitude cut (2, 5 mag). For isotropic spectral templates, we used 3 isotropic spectral templates and the corresponding instrument response function, `iso_P8R3_SOURCE`, `iso_P8R3_CLEAN` and `iso_P8R3.UNTRACLEANVETO` along with their corresponding the event class and event type. The other two have larger effective areas at the expense of higher contamination of background events. By testing different combinations of these templates, we found that the error introduced by background selection was below 25%, with the detection significance (the TS value) ranging from 23.52 to 28.39 for the source W and from 45.72 to 62.25 for the disk component.

We summarize the results on systematic uncertainties in Table 3. The largest uncertainty in the photon flux arises from the uncertainty in the Galactic diffuse foreground, while other effects have only minor influence.

B. SEARCH FOR RADIO SOURCES IN THE ERROR BOX OF THE SOURCE W

We study whether there is any counterpart to the source W. Since most of the gamma-ray-emitting AGNs are sources of radio emission, we search for possible radio sources within 0.12° (99% containment radius) around the point-like source in the radio source catalogs of SIMBAD Astronomical Database⁴ and NASA/ IPAC EXTRAGALACTIC DATABASE (NED)⁵. There are no AGNs within 0.12° . A bright radio AGN (7C 124442.50+275745.00) with a flux density of 178 mJy is located beyond the 99% containment radius given by the *source_localization* tool implemented in *Fermipy*, so we think this source is irrelevant to the source W. We also check the flat-spectrum radio source catalog, CRATES⁶. No source is found within our 99% containment radius.

In our search for possible X-ray counterparts in the eROSITA DR1 catalog⁷, we found a X-ray point source, 1eRASS J124657.2+272806, within the 1σ positional error of the source W, with a flux of $1.2 \times 10^{-13} \text{ erg cm}^{-2} \text{ s}^{-1}$. Additionally, by comparing this region with data from the VLASS survey⁸, we note the presence of a radio point source, VLASS1QLCIR J124657.34+272759.6, within the 2σ positional uncertainty region of the eROSITA X-ray

⁴ <http://simbad.cds.unistra.fr/simbad>

⁵ <https://ned.ipac.caltech.edu/forms/nearposn.html>

⁶ <https://heasarc.gsfc.nasa.gov/W3Browse/radio-catalog/crates.html>

⁷ <https://erosita.mpe.mpg.de/dr1/erodat/>

⁸ <https://science.nrao.edu/vlass>

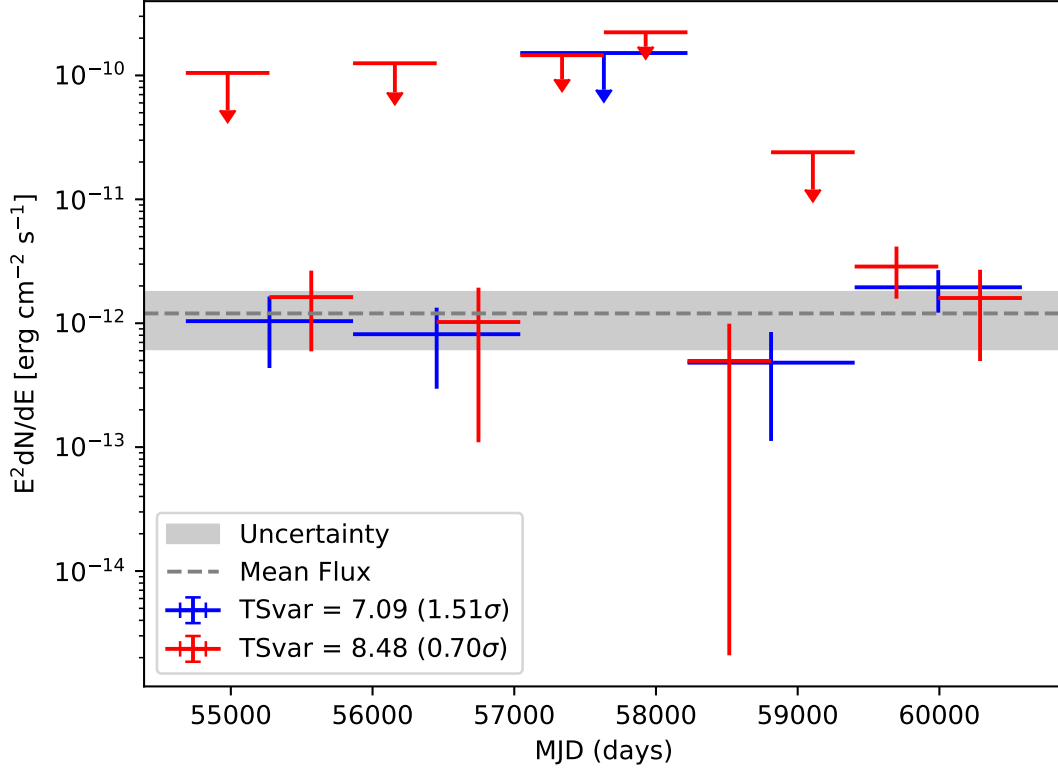


Figure 4. Light curves of the source W with five and ten time bins. The mean flux is the averaged flux over 16.2 yr. The upper limits at the 95% confidence level are derived when the TS value for the data points is lower than 4.

source, with a flux density of 1.4 mJy in the 2–4 GHz band. According to the radio-GeV flux correlation for *Fermi* blazars (Ghirlanda et al. 2011), the expected GeV flux of this radio source is insufficient to account for the GeV flux of source W, although we cannot completely rule out the possibility of the association between two sources considering the uncertainty in the radio-GeV correlation.

C. FLUX VARIABILITY OF THE SOURCE W

We retained the point-source model at the best-fit location for examining the variability of the gamma-ray flux. We computed light curves in five and ten time bins using 16.2 years of *Fermi*-LAT data, for events in the energy range 0.1–1000 GeV. For the analysis in each time bin, all sources within the 6° region around the source W have their spectra fixed to the shapes obtained from the above broadband analysis. The result is shown in Fig. 4. We then used a likelihood-based statistic to test the significance of the variability. Following the definition in 2FGL Nolan et al. (2012), the variability index from the likelihood analysis is constructed, with a value in the null hypothesis where the source flux is constant across the full time period, and the value under the alternate hypothesis where the flux in each bin is optimized: $TS_{\text{var}} = 2 \times \sum_{i=1}^N [\log(\mathcal{L}_i(F_i)) - \log(\mathcal{L}_i(F_{\text{mean}}))]$ (\mathcal{L}_i is the likelihood corresponding to bin i , F_i is the best-fit flux for bin i , and F_{mean} is the best-fit flux for the full time) Nolan et al. (2012). We find a 0.7–1.5 σ significance for the flux variability for the analyses using the above two time bins, which suggests no significant variability for the gamma-ray emission from the source W.

REFERENCES

- | | |
|---|--|
| Ackermann, M., Ajello, M., Atwood, W. B., et al. 2012, <i>ApJ</i> , 750, 3, doi: 10.1088/0004-637X/750/1/3 | Adam, R., Goksu, H., Brown, S., Rudnick, L., & Ferrari, C. 2021, <i>A&A</i> , 648, A60, doi: 10.1051/0004-6361/202039660 |
| Ackermann, M., Ajello, M., Albert, A., et al. 2016, <i>ApJ</i> , 819, 149, doi: 10.3847/0004-637X/819/2/149 | Baghmany, V., Zargaryan, D., Aharonian, F., et al. 2022, <i>MNRAS</i> , 516, 562, doi: 10.1093/mnras/stac2266 |

- Ballet, J., Bruel, P., Burnett, T. H., Lott, B., & The Fermi-LAT collaboration. 2023, arXiv e-prints, arXiv:2307.12546, doi: [10.48550/arXiv.2307.12546](https://doi.org/10.48550/arXiv.2307.12546)
- Bonafede, A., Brunetti, G., Rudnick, L., et al. 2022, ApJ, 933, 218, doi: [10.3847/1538-4357/ac721d](https://doi.org/10.3847/1538-4357/ac721d)
- Brown, S., & Rudnick, L. 2011, MNRAS, 412, 2, doi: [10.1111/j.1365-2966.2010.17738.x](https://doi.org/10.1111/j.1365-2966.2010.17738.x)
- Brunetti, G., & Jones, T. W. 2014, International Journal of Modern Physics D, 23, 1430007, doi: [10.1142/S0218271814300079](https://doi.org/10.1142/S0218271814300079)
- Enßlin, T. A., Lieu, R., & Biermann, P. L. 1999, A&A, 344, 409, doi: [10.48550/arXiv.astro-ph/9808139](https://doi.org/10.48550/arXiv.astro-ph/9808139)
- Ghirlanda, G., Ghisellini, G., Tavecchio, F., Foschini, L., & Bonnoli, G. 2011, MNRAS, 413, 852, doi: [10.1111/j.1365-2966.2010.18173.x](https://doi.org/10.1111/j.1365-2966.2010.18173.x)
- Ha, J.-H., Ryu, D., & Kang, H. 2023, ApJ, 943, 119, doi: [10.3847/1538-4357/acabbe](https://doi.org/10.3847/1538-4357/acabbe)
- Keshet, U., Kushnir, D., Loeb, A., & Waxman, E. 2017, ApJ, 845, 24, doi: [10.3847/1538-4357/aa794b](https://doi.org/10.3847/1538-4357/aa794b)
- Keshet, U., & Reiss, I. 2018, ApJ, 869, 53, doi: [10.3847/1538-4357/aaeb1d](https://doi.org/10.3847/1538-4357/aaeb1d)
- Keshet, U., Waxman, E., Loeb, A., Springel, V., & Hernquist, L. 2003, ApJ, 585, 128, doi: [10.1086/345946](https://doi.org/10.1086/345946)
- Kushnir, D., & Waxman, E. 2010, JCAP, 2010, 025, doi: [10.1088/1475-7516/2010/02/025](https://doi.org/10.1088/1475-7516/2010/02/025)
- Loeb, A., & Waxman, E. 2000, Nature, 405, 156, doi: [10.1038/35012018](https://doi.org/10.1038/35012018)
- Miniati, F. 2003, MNRAS, 342, 1009, doi: [10.1046/j.1365-8711.2003.06647.x](https://doi.org/10.1046/j.1365-8711.2003.06647.x)
- Miniati, F., Jones, T. W., Kang, H., & Ryu, D. 2001, ApJ, 562, 233, doi: [10.1086/323434](https://doi.org/10.1086/323434)
- Miniati, F., Ryu, D., Kang, H., et al. 2000, ApJ, 542, 608, doi: [10.1086/317027](https://doi.org/10.1086/317027)
- Nolan, P. L., Abdo, A. A., Ackermann, M., et al. 2012, ApJS, 199, 31, doi: [10.1088/0067-0049/199/2/31](https://doi.org/10.1088/0067-0049/199/2/31)
- Pfrommer, C., & Jonathan Dursi, L. 2010, Nature Physics, 6, 520, doi: [10.1038/nphys1657](https://doi.org/10.1038/nphys1657)
- Pfrommer, C., Springel, V., Enßlin, T. A., & Jubelgas, M. 2006, MNRAS, 367, 113, doi: [10.1111/j.1365-2966.2005.09953.x](https://doi.org/10.1111/j.1365-2966.2005.09953.x)
- Pinzke, A., & Pfrommer, C. 2010, MNRAS, 409, 449, doi: [10.1111/j.1365-2966.2010.17328.x](https://doi.org/10.1111/j.1365-2966.2010.17328.x)
- Ryu, D., Kang, H., Hallman, E., & Jones, T. W. 2003, ApJ, 593, 599, doi: [10.1086/376723](https://doi.org/10.1086/376723)
- Scharf, C. A., & Mukherjee, R. 2002, ApJ, 580, 154, doi: [10.1086/343035](https://doi.org/10.1086/343035)
- Thierbach, M., Klein, U., & Wielebinski, R. 2003, A&A, 397, 53, doi: [10.1051/0004-6361:20021474](https://doi.org/10.1051/0004-6361:20021474)
- Totani, T., & Kitayama, T. 2000, ApJ, 545, 572, doi: [10.1086/317872](https://doi.org/10.1086/317872)
- van Weeren, R. J., de Gasperin, F., Akamatsu, H., et al. 2019, SSRv, 215, 16, doi: [10.1007/s11214-019-0584-z](https://doi.org/10.1007/s11214-019-0584-z)
- Xi, S.-Q., Wang, X.-Y., Liang, Y.-F., et al. 2018, PhRvD, 98, 063006, doi: [10.1103/PhysRevD.98.063006](https://doi.org/10.1103/PhysRevD.98.063006)